# Synthesis and characterization of bolaform surfactants from sugar derivative and their associates with 2-aminobenzimidazole as inhibitor of zinc in 3% NaCl medium

Adil El Yadini, H Saufi, Emile Perez, Muriel Blanzat, Sophie Franceschi-Messant, Souad El Hajjaji

# Synthesis and characterization of bolaform surfactants from sugar derivative and their associates with 2-aminobenzimidazole as inhibitor of zinc in 3% NaCl medium

**A. El Yadini,[1,2] H. Saufi,[1] E. Perez,[2] M. Blanzat,[2] S. Franceschi-Messant[2] and S. El Hajjaji[1]***

*[1]Laboratory of Spectroscopy, Molecular Modeling, Materials, Nanomaterials, Water and Environment, CERNE2D, Faculty of science, Mohammed V University in Rabat, Morocco*
*[2]Laboratoire des Interactions Moléculaires et Réactivité Chimique et Photochimique UMR 5623, 118 route de Narbonne – 31062, Toulouse, Cedex – France*
**E-mail: souad.elhajjaji@fsr.um5.ac.ma*

## Abstract

The purpose of this manuscript is to synthesize and characterize new corrosion inhibitor compounds such as ion paired surfactants (1,7-lactobionamidoheptanoic acid) derived from non-toxic soluble sugars and to examine the inhibitory effect of these products on the corrosion of zinc in the 3% NaCl medium. The prepared products are chemically pure, and the average yield is of the order of 80%. The characterization of these molecules was performed by NMR ($^{1}$H and $^{13}$C), IR, mass spectroscopy and elementary analysis. The anticorrosive effect of the surfactant, (1,7-lactobionamidoheptanoic acid) on the corrosion of zinc in 3% NaCl solution was evaluated by gravimetric and electrochemical techniques (potentiodynamic polarization and electrochemical impedance spectroscopy). The results showed that our synthesized surfactant (the bolaform: 1,7-lactobionamidoheptanoic acid) is an excellent corrosion inhibitor for zinc in 3% NaCl. Up to 90% inhibitory efficacy has been demonstrated by surfactant at a concentration of $5 \cdot 10^{-3}$ M. Based on polarization curves, it is clear that the surfactant 1,7-lactobionamidoheptanoic acid can be considered as a mixed inhibitor with a predominantly cathodic character. Inhibitory efficacy increases with increasing inhibitor concentration. No corrosion product formed.

Received: March 30, 2022. Published: January 3, 2023 doi: 10.17675/2305-6894-2023-12-1-2

***Keywords:*** *organic compounds, ion paired surfactants, 1, 7-lactobionamidoheptanoic acid, bolaform, corrosion inhibition.*

## Introduction

It is well known that the high affinity of surfactant molecules to adsorb on to interfaces is responsible for their applications in several interfacial systems. Consequently, surfactants can be used as good corrosion inhibitors in metallic surfaces [1].

Surfactants are among the most versatile materials used in many applications [2]. Thus, they have been used worldwide in large quantities everyday as detergents, petroleum

additives, antibacterial [3, 4], liquid crystals [5], gene transfection agents [6], road repair materials [7], mineral flotation agents [8], metal protection corrosion [9, 10], phase transfer catalysts in regioselective addition reactions [11, 12] and in preparation of crystalline mesoporous materials [13, 14]. As a result, demands for high-performance surfactants are continuously increasing.

Classical surfactant molecules are generally composed by two distinct chemical parts: a polar head and an alkyl chain. These two parts are incompatible. For instance, this self-association affords a unique molecular architecture assembly, called micelle [15].

Great numbers of scientific studies have been devoted to the application of surfactants as metal corrosion inhibitors [16–19]. It was found that organic surfactants inhibit corrosion by forming an adsorbed film at the metal-electrolyte interface. The film formation results either from the weakly bonded and physisorbed ions or molecules, or from strongly bonded and chemisorbed species, depending on the characteristics of both the metal surface and the surfactant.

The surfactants may inhibit either the cathodic or the anodic reactions, or in some cases both. However, there is no strict proof about the nature of the adsorbed film, the mechanism of adsorption and its specific role in retarding the electrode reaction. An inhibitory augmenting action was observed when the concentration of the surfactant in the corrosive solution is close to the critical micelle concentration (CMC) [20].

In the present work, we synthesized 1,7-lactobionamidoheptanoic acid (L6). This bolaform was associated with 2-aminobenzimidazole to form an ion pair: bolaform/benzimidazole. The formed surfactant is soluble in water and has been successively identified and characterized by different techniques which include NMR, IR, mass spectrum and microanalysis. In order to examine the capacity of this surfactant to inhibit corrosion on metallic surface (1 $cm^2$), gravimetric and Kesternich assays were performed over zinc plate in 3% NaCl.

## Experimental

All chemicals used in the investigation were purchased from Aldrich Chemical, France. Corrosion tests by gravimetry were performed in 3% NaCl solutions, immersion was performed for 7 days, and the samples were dried and weighed every 24 h.

### *Electrochemical investigation*

Electrochemical experiments were performed in aerated solution of 3% NaCl by means of potentiostatic technique. The cell contains a platinum disc as counter electrode, a saturated calomel electrode as reference and the working electrode (zinc). Before every run, the surface of the electrode was abraded using emery paper of 1200 grades until it is mirror bright. The potential scanning rate was 500 μV/s. The polarization curves of zinc were recorded in the absence and presence of different concentrations of the inhibitor after 20 min.

The electrochemical impedance spectroscopy (EIS) was carried out with a Tacussel electrochemical system which included a digital potentiostat model Voltalab PGZ 301

computer at $E_{corr}$ after immersion in solution without bubbling, the circular surface of zinc exposing of 1 $cm^2$ to the solution were used as working electrode. After the determination of steady-state current at a given potential, sine wave voltage (10 mV) peak to peak, at frequencies between 100 kHz and 10 mHz were superimposed on the rest potential. Computer programs automatically controlled the measurements performed at rest potentials after 60 min of exposure. The impedance diagrams are given in the Nyquist and Bode representations. The fitting parameters were obtained using the EC-Lab software.

*Inhibitor synthesis and characterization*

*NMR spectrum*

$^1H$ and $^{13}C$ NMR spectra were recorded on Bruker Advance 300 spectrometer at nominal frequencies of 300.18 MHz for $^1H$ and 75.48 MHz for $^{13}C$, respectively.

*Infrared spectrum*

Infrared spectra were recorded on a Perkin-Elmer FT 1760-X spectrometer (0.5% KBr).

*Mass spectrum*

A Waters Q-T of Ultima API mass spectrometer with an electrospray ionisation source (ESI) in positive mode was used for HRMS measurement. The capillary, cone and *Rf* lens potentials were set to 3 kV, 35 and 40 V, respectively. The source and desolvation temperature were set to 100 and 120°C and the collision energy was 10 eV in TOF–MS mode. Analyses were monitored with MassLynx 4.0 software. To measure the exact mass of the catanionic associations, the spectrometer was calibrated with $H_3PO_4$ clusters.

*Synthesis of the associate of 1,7-lactobionamidoheptanoic acid (L6) with 2-aminobenzimidazole*

In 20 mL of pure water, we introduced 200 mg of 2-aminobenzimidazole and 759 mg of 1,7-lactobioamidoheptanoic acid (L6). The reaction mixture was stirred at 50°C for 24 h, and then freeze-dried. A white solid was collected (Figure 1, Figure 2 and Figure 3).

ρ=73% (flash chromatography, *Rf*=0.4).

$^1H$ NMR (300 MHz, $D_2O$) δ ppm: 1.27 (m, 4H, $C_{14,15}$–H); 1.48 (m, 4H, $C_{13,16}$–H); 2.31 (t, 2H, $C_{17}$–H); 2.81–3.01+3.47–3.89 (m, 10H, $C_{21–24,27–30}$–H); 3.18 (t, 2H, $C_{12}$–H); 3.89 (1H, $C_{26}$–H); 4.27 (d, 1H, $C_{20}$–H); 5.19 (d, 1H, $C_{25}$–H); 7.22 (dd, 2H, $C_{7,6}$–H); 7.83 (d, 2H, $C_{5,8}$-H (aromatic ring); 7.98 (3H, $NH_3^+$).

The proton bound to carbon 15 is more deshielded because of the inductive effect of attractor two oxygens, bound to carbon 10 is at most deshielded by the attractor inductive effect of oxygen and the mesomeric attractor carbonyl.

The proton bound to carbon 7 is more deshielded compared to the proton bound to the carbon 2 as oxygen binds to the carbon bearing the proton has a significant effect that the attractor carbonyl.

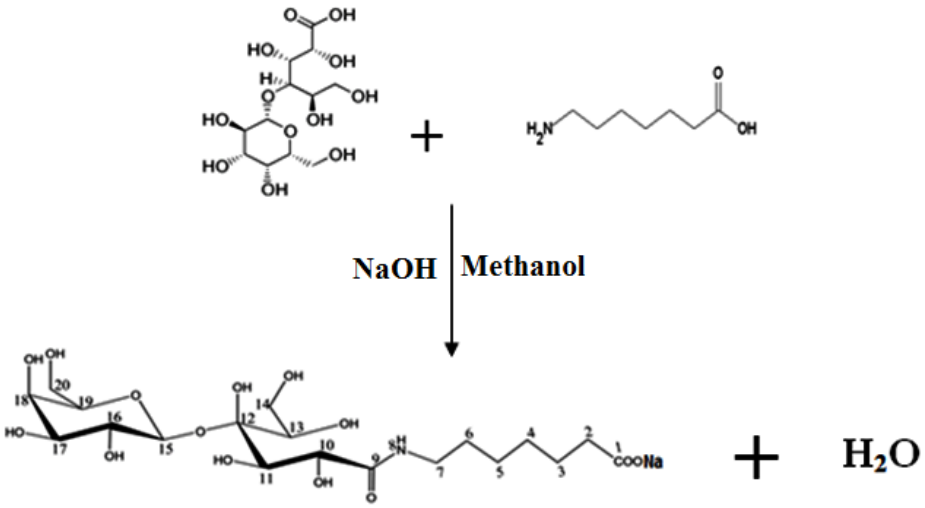


**Figure 1.** Synthesis of 1,7-lactobionamidoheptanoate (L6Na).

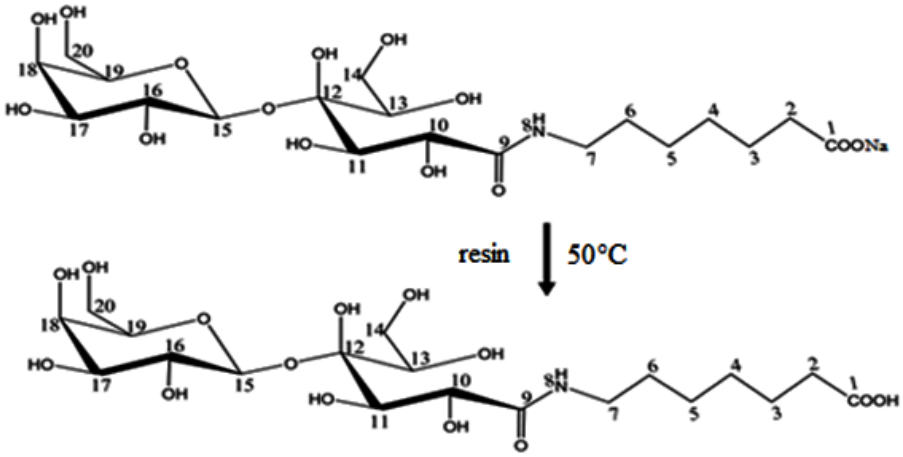


**Figure 2.** Synthesis of 1,7-lactobionamidoheptanoic acid (L6).

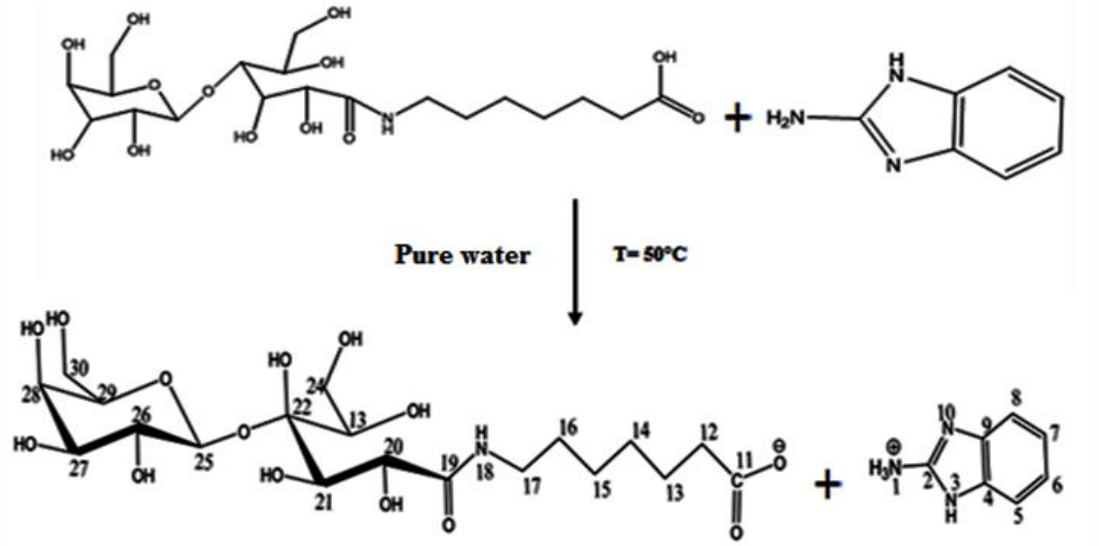


**Figure 3.** Association of 1,7-lactobionamidoheptanoic acid (L6) with 2-aminobenzimidazole.

$^{13}C$-{$^{1}H$} NMR (75 MHz, $D_2O$) δ ppm: 25.33–26.10 ($C_{14}$ and $C_{15}$); 28.48–30.84 ($C_{13}$ and $C_{16}$); 37.13 ($C_{12}$); 39.89 ($C_{17}$); 62.26–64.25 ($C_6$ and $C_{6'}$); 69.77–70.54–71.34–73.65–74.85–76.44 ($C_{21}$, $C_{22}$, $C_{23}$, $C_{24}$, $C_{27}$, $C_{28}$, $C_{29}$, $C_{30}$); 77.60 ($C_{26}$); 81.54 ($C_{20}$); 108.67 ($C_{25}$); 117.31 ($C_6$, $C_7$); 124.77 ($C_5$, $C_8$); 139.71 ($C_4$, $C_9$); 142.86 ($C_2$); 173.53 ($C_{19}$); 183.74 ($C_{11}$).

The carbon 15 is more deshielded because of the inductive effect of attractor two oxygens and the carbon 10 is at most deshielded by the attractor inductive effect of oxygen and the mesomeric attractor carbonyl.

The carbon 7 is more deshielded compared to the carbon 2, since nitrogen bound to the carbon that bears that proton has a significant effect that the attractor carbonyl. The first acid carbonyl is more deshielded than the carbonyl of the amide 9.

- IR (KBr) $cm^{-1}$: 1647 ($\nu_{C=O}$ (amide)); 183.46 ($\nu_{COO^-}$).
- ESI: $m/z$=619 $[M+H]^+$; M = 2-aminobenzimidazole+1,7-lactobioamidoheptanoic acid.
- Elemental analysis: C%: 50.48, H%: calculated: 6.84; N%: 9.06; found: C%: 49.97, H%: 6.20, N%: 8.94.

*Dynamic light scattering (DLS)*

The size of the vesicles was evaluated in aqueous solution by dynamic light scattering (DLS) using a Malvern Instrument Zetasizer 3000HR equipped with a 5 mW helium–neon laser with an output wavelength of 633 nm. The scattering angle was 90º and the intensity autocorrelation actions were analyzed using the Automatic method. This system was able to be used for samples containing particles from 5 nm to 10 nm. The polydispersity index (PI) obtained from this type of experiment renders the vesicle size distribution [21]. The higher the polydisperse index is, the more important is the amplitude of the diameter distribution. Vesicles are considered as monodisperse for PI/0.66. The formation of the vesicles was observed through Transmission Electron Microscopy (TEM) using a JEOL JEM 1011 electron microscope, operating at 80 kV. Mixtures of associations in water were applied on copper grids (Formvar), negatively stained with a 2% (wt/vol) of sodium phosphotungstate (pH 7.5).

*Surface analyses*

The surface morphology of the samples, after immersion in 3% NaCl solution containing inhibitor or not, was investigated by MEB-EDS.

## Results and Discussion

*Ion-pair synthesis*

The synthesis of the sugar-based bolaamphiphile is based on a two-step synthesis already described in the literature. After reaction between the long chain aminoacid and lactobionic acid in a basic medium, the carboxylic acid function is regenerated using an ion-exchange resin (Figure 3). Then the synthesis of the ion-pair was achieved using an acid-base reaction

in water between stoichiometric amounts of the sugar-derived bolaamphiphile and 2-aminobenzimidazole. This method easily and quantitatively led to the water-soluble ion-pair.

All the associations were fully characterized by $^{1}$H NMR, $^{13}$C NMR and FT-IR spectroscopy. The completion of the reaction is characterized by the complete disappearance of the carboxylic absorption band at 1724 $cm^{-1}$ and appearance of the carboxylate stretching symmetric and asymmetric bands respectively at 1402.4 $cm^{-1}$ and 1568.6 $cm^{-1}$.

*Determining the CMC (critical micelle concentration)*

We determined the wavelength of our synthesized product at a definite concentration ($10^{-3}$ M) and we found λ=280 nm. Then we prepared diluted solutions, to plot the curve of absorbance versus the concentration (Figure 4).

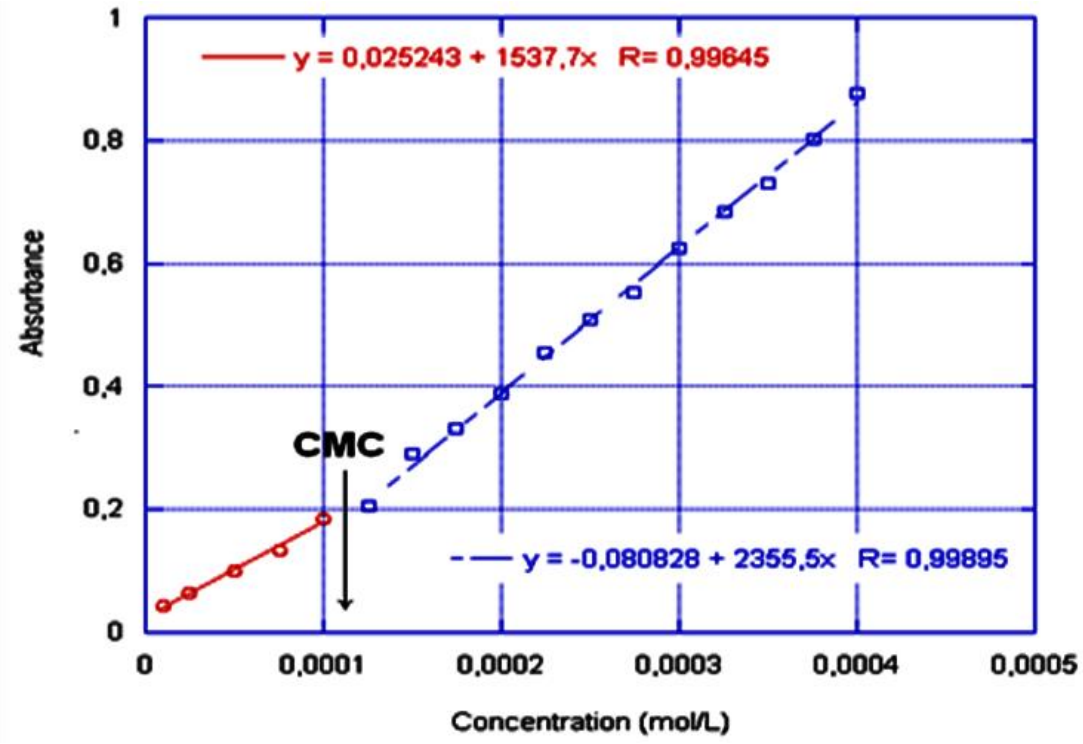


**Figure 4**. Determination of the CMC of the surfactant: 1,7-lactobioamidoheptanoic acid (L6)+2-aminobenzimidazole.

Therefore, we deduce the value of the CMC from the intersection of two curves, which is of the order of $1.2\times10^{-3}$ mol/L.

*Analysis by DLS (quasi-elastic scattering of light)*

We prepared solutions containing 1,7-lactobionamidoheptanoic acid (L6) and (1,7-lactobionamidoheptanoic acid (L6)+2-aminobezimidazole) at a concentration above the critical micelle concentration, then we analyzed these samples by DLS in order to examine the existence of aggregates or objects in these solutions (Table 1).

**Table 1.** Analysis by DLS and the (bolaform) and (bolaform + 2-aminobezimidazole) in 3% NaCl and water.

| Products | Diam/NaCl (nm) | Diam/water (nm) |
|---|---|---|
| Bolaforme | 59.64 | 43.41 |
| Bolaforme + 2-aminobezimidazole | 63.03 | 88.87 |

DLS analysis of these solutions has shown the existence of objects whose size varied in presence of NaCl and water.

In the NaCl solution, we notice that the diameter of the formed object of the bolaform (1,7-Lactobionamidoheptanoic Acid (L6)) (59.64 nm) is larger than the one formed in water (43.41 nm). In the water, we notice that the diameter of the formed object of the associated bolaform (1,7-Lactobionamidoheptanoic Acid (L6) + 2-aminobenzimidazole) (88.87 nm) is larger than the one formed in NaCl (63.03 nm). These vesicles were only stable for a few hours.

*Gravimetric measurements*

The gravimetric measurements corroborate the electrochemical results. The inhibitor efficiency, *IE*(%), was also estimated from weight loss measurements using the relation (1):

$$IE(\%) = \frac{W - W_{\text{inh}}}{W} \cdot 100 \quad (1)$$

where $W$ and $W_{\text{inh}}$ are rate of corrosion ($g \cdot cm^{-2}\ h^{-1}$) with and without inhibitor, respectively. Corresponding data are given in Table 2, for immersion period of 7 days.

**Table 2.** The corrosion rates in the absence and presence of inhibitor in 3% NaCl and inhibitor efficiency *IE*(%) determined by gravimetric method.

| Inhibitor | Corrosion rate ($g \cdot cm^{-2} \cdot h^{-1}$) | *IE* (%) |
|---|---|---|
| Blank | 0.260 | – |
| NaCl 3% + (Bolaform $10^{-3}$ M) | 0.195 | 25 |
| NaCl 3% + (Bolaform + 2-aminobenzimidazol $10^{-3}$ M) | 0.028 | 89 |

Figure 5 represents the data of weight loss time curves for the system involving inhibitor or not.

The samples of zinc were immersed in 3 solutions of 3% NaCl each one contains a different molecule. After 7 days of immersion, we calculated and plotted the curves of mass loss. The results of gravimetric measurements are shown in Figure 5.

Figure 5 show that there is a slight decrease of the mass of zinc in the solution (3) (3% NaCl + (1,7-lactobionamidoheptanoic acid (L6) + 2-aminobenzimidazole) compared to

the other solutions (1) (3% NaCl) and (2) (3% NaCl+1,7-lactobionamidoheptanoic acid (L6)).

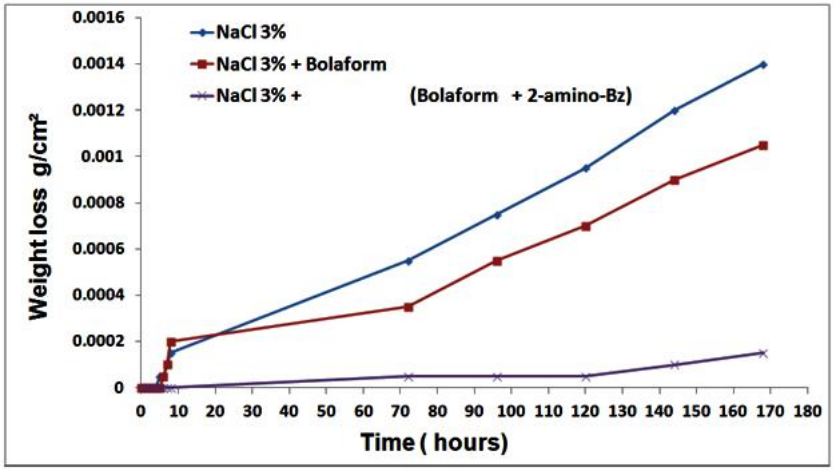


**Figure 5.** Influence of 3% NaCl medium on iron in the absence and presence of different molecules studied.

To determine the efficiency of these inhibitors, we calculated the corrosion rate in 3% NaCl solution. Corresponding data are given in Table 2.

The inhibitors efficiency was estimated to be 89% for inhibitor (bolaform+2-aminobenzimidazole: (B+Bz)) and 25% for inhibitor bolaform. Thus, we deduce that the inhibitor (B+Bz) has a better efficiency compared to the other inhibitor.

*SEM observation*

Figure 6 displays the surface state of zinc, observed by SEM analysis, after immersion in 3% NaCl solution alone or even with other inhibitors (Bolaforme, Lactobionic acid, Lactobionic acid + 2-aminobenzimidazole). The presence of rust on the surface of sample shows clearly that zinc has undergone corrosion. On the other hand, in the presence of the inhibitor Bolaforme+ 2-aminobenzimidazole, the surface of zinc immersed in 3% NaCl medium is fond homogeneous with an absence of zinc oxide ZnO, which may be produced by corrosion.

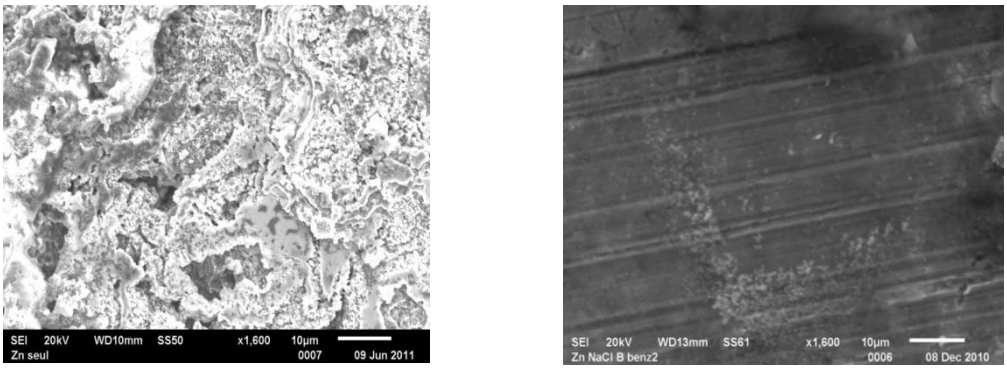


**Figure 6.** Micrographs showing surface of zinc after gravimetric test in 3% NaCl solution.

*Kesternich test*

Cycles are programmed with duration of 24 h each. Kesternich cycle consists of two steps:

- 6 h at 40°C in total moisture;
- 18 h at 25°C without humidity;

The samples are weighed before and after each cycle in order to obtain an average value of mass uptake (mg/dm²). The weighing of each plate was made during 1 h, 4 h, 8 h, 24 h and 72 h. Then we analyzed these samples by the Kesternich test to examine the adsorption of molecules on the surface of the zinc. The results are presented in Figures 7 and 8.

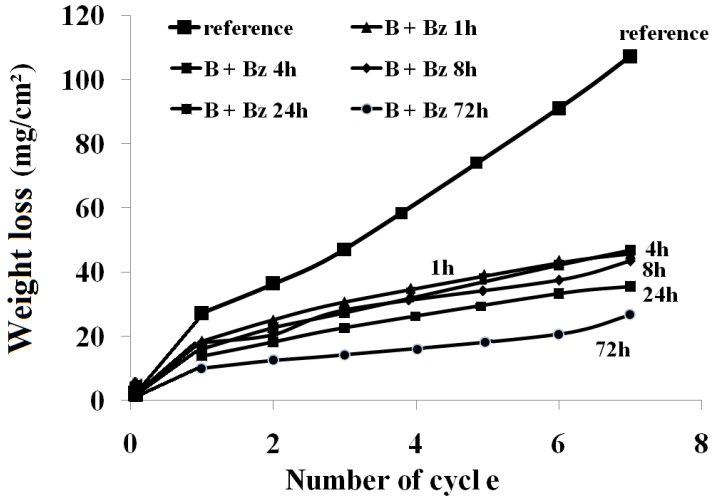


**Figure 7.** Kesternich Test on the plates of zinc in the presence of inhibitor (B+Bz).

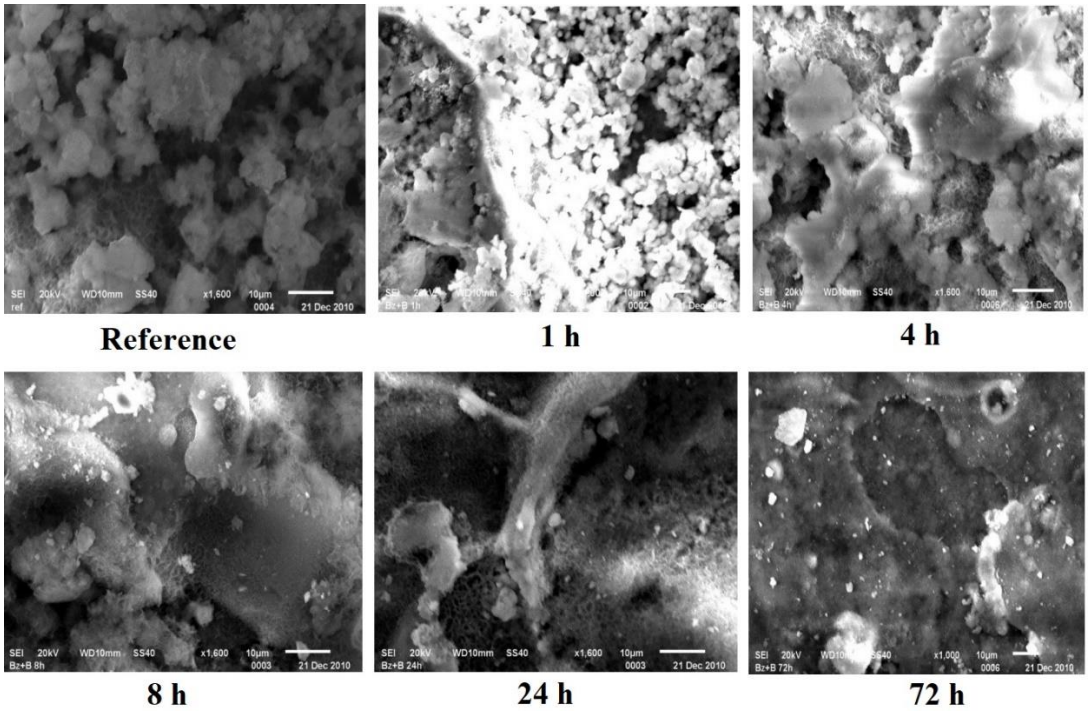


**Figure 8.** Micrographs showing surface of zinc after Kesternich test in 3% NaCl solution.

The longer the period of the immersion of the zinc (72 h) in a solution that contains the inhibitor (B+Bz), the lower the mass uptake will be.

*Electrochemical testing*

The polarization curves of zinc sample in the absence and presence inhibitor are presented in Figure 9 and 10. The corrosion potential ($E_{corr}$) was found to be –1377 mV/ECS ($5 \cdot 10^{-3}$ M of inhibitor). The corrosion current density can be obtained from the extrapolation of Tafel line to the corrosion potential; in the present work it was found to be 7.36 mA/cm² ($5 \cdot 10^{-3}$ M of inhibitor). The inhibitor efficiency was estimated to be 93.1% for inhibitor ($5 \cdot 10^{-3}$ M). These results were calculated using the following expression (2) [22]:

$$IE(\%) = \frac{I_{corr} - I_{corr(inh)}}{I_{corr}} \cdot 100 \quad (2)$$

where $I_{corr}$ and $I_{corr(inh)}$ are respectively the corrosion current densities without and with inhibitor, respectively, evaluated by extrapolation of Tafel lines to the corrosion potential. The corrosion parameters $I_{corr}$, $E_{corr}$ and inhibitor efficiency, *IE*%, obtained in uninhibited and inhibited solutions are given in Table 3. The higher corrosion resistance was exhibited by the zinc samples in the presence of inhibitor B+Bz ($5 \cdot 10^{-3}$ M).

According to Tafel lines, we observed a shift of potential towards more negative values in cathode region and a diminution of the current density towards negative values. Thus, we deduce that we have a mixed inhibitor.

Analysis of polarization curves allowed us to define the electrochemical parameters and inhibition efficiency of corrosion of zinc in 3% NaCl without and with addition of different concentrations of the inhibitor (Table 3).

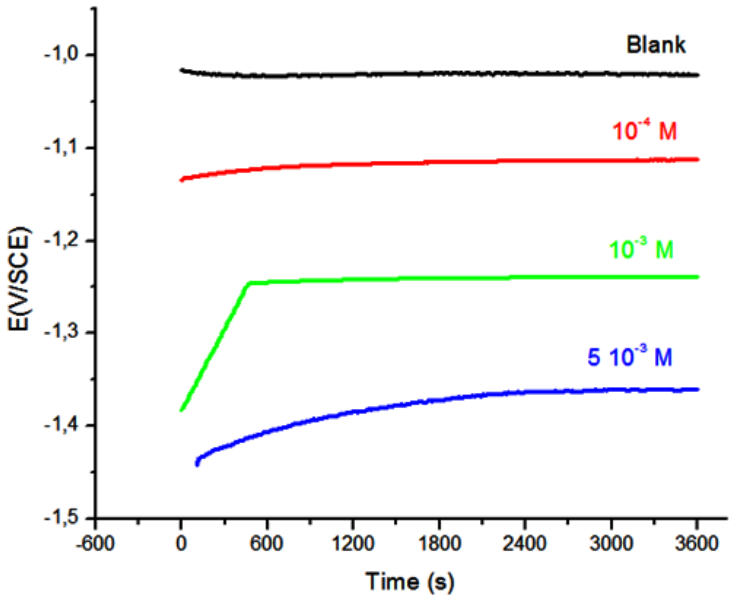


**Figure 9.** Electrode potential as a function of time (chronopotentiogram) of zinc in 3%NaCl in the absence and presence of different concentrations of inhibitor.

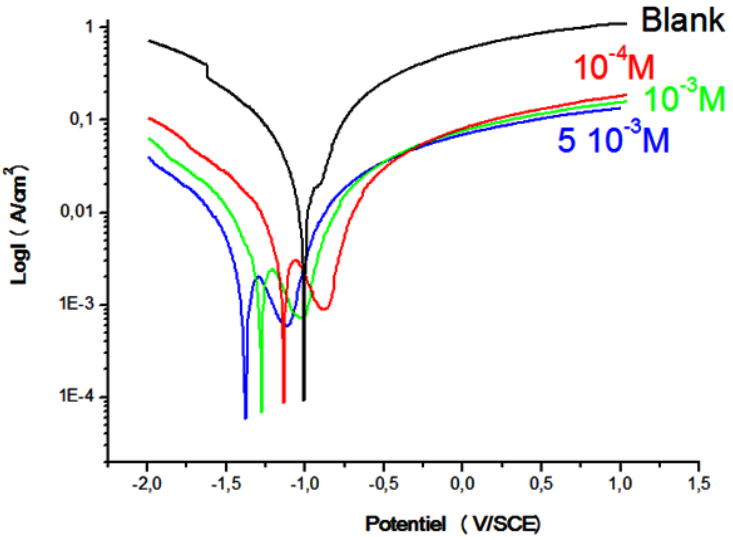


**Figure 10.** Polarization curves of zinc in 3% NaCl in the absence and presence of different concentrations of the inhibitor.

**Table 3.** Electrochemical parameters ($E_{corr}$ and $I_{corr}$) and inhibitor efficiency (*IE*%), of the zinc in 3% NaCl solution with and without inhibitor.

| Inhibitor | $E_{corr}$ (mV) | $I_{corr}$ (mA/cm²) | *IE*% |
|---|---|---|---|
| Blank | –1010 | 107.05 | – |
| NaCl 3%+B+Bz ($10^{-4}$) | –1142 | 12.45 | 88.3 |
| NaCl 3% B+Bz ($10^{-3}$) | –1283 | 9.25 | 91.3 |
| NaCl 3% B+Bz ($5\cdot10^{-3}$) | –1330 | 7.36 | 93.1 |

*Electrochemical impedance spectroscopy*

Electrochemical impedance spectroscopy (EIS) measurements have been carried out at 298 K in 3% NaCl solution with and without B+Bz compound at the corresponding open-circuit potentials. The Nyquist and Bode plots (Figures 11 and 12) obtained, for zinc in 3% NaCl medium containing different concentrations of B+Bz, show two phenomena as seen in the literature for NaCl media [23, 25].

The two observed phenomena are two capacitive loops, one for the charge transfer and the second one for the passive layer of the products of corrosion [23]. Therefore, we used the equivalent circuit shown in Figure 13 to fit our experimental impedance data. The constant phase element (CPE) is substituted for the capacitive element to give a more accurate fit as specified in the CPE impedance, equation 3 [24].

$$Z_{CPE} = Q^{-1}(i\omega)^{-\eta} \quad (3)$$

where $Q$ is the CPE constant, ω is the angular frequency (in rad·s$^{-1}$), $i^2=-1$ is the imaginary number and, is a CPE exponent. All the impedance parameters obtained from the

experimental impedance data fit, including $R_1$, $R_2$, $Q$ and η, are shown in Table 4. The calculated inhibition efficiency according to the equation 4 is also given in Table 4.

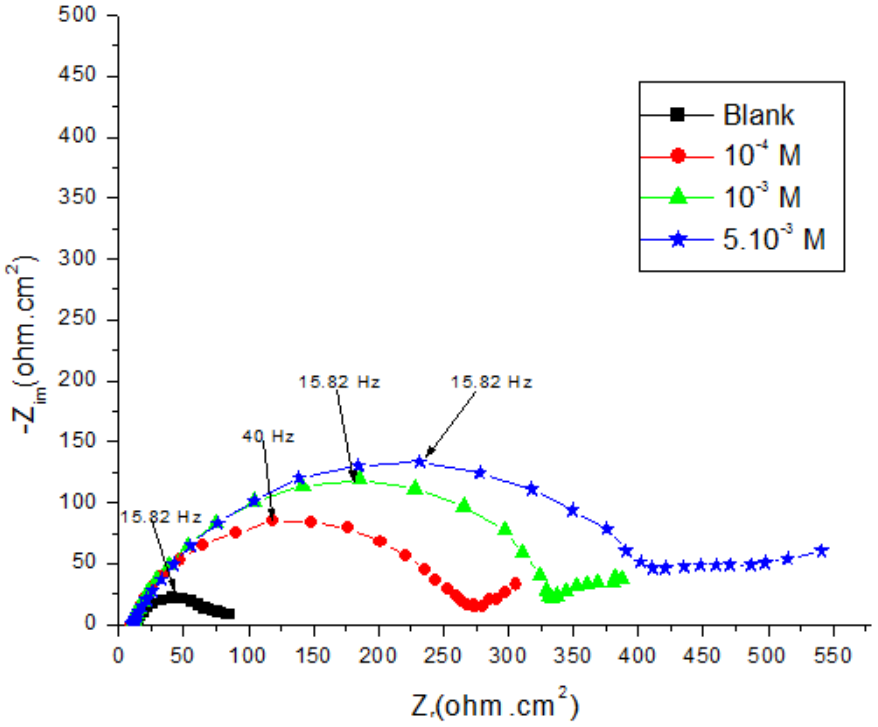


**Figure 11.** Nyquist plots of zinc in 3% of NaCl solution containing various concentrations.

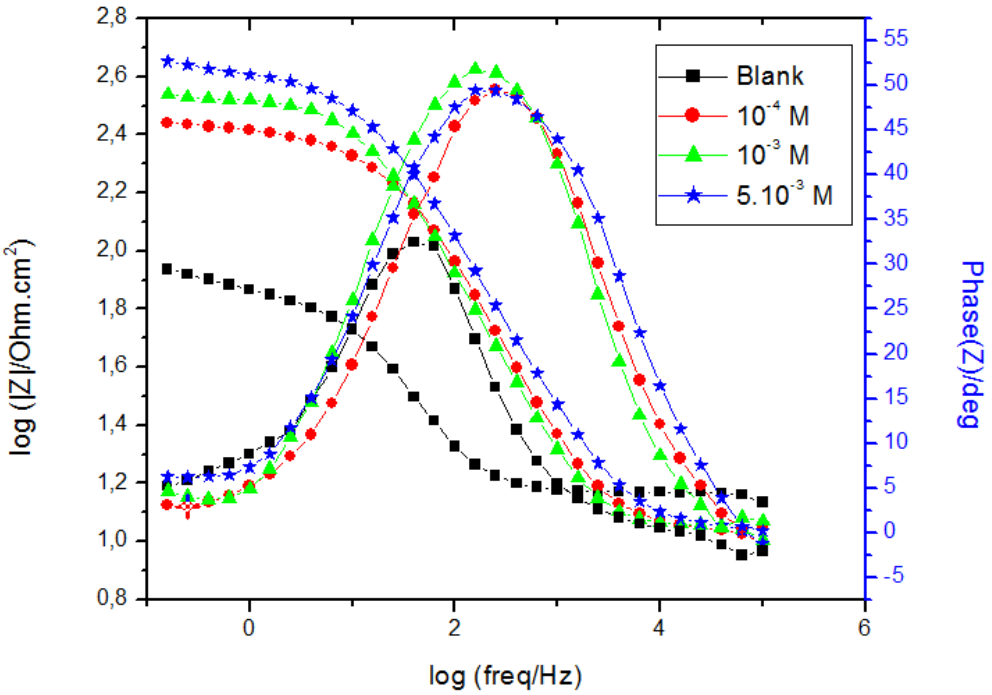


**Figure 12.** The Bode modulus and Bode phase of zinc substrate immersed for 1h in 3% NaCl.

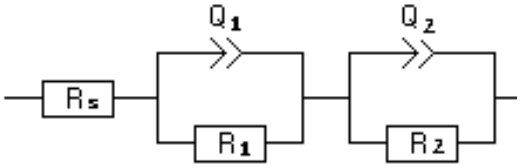


**Figure 13.** The equivalent circuit used for impedance spectra fitting.

**Table 4.** Electrochemical parameters and inhibitory efficiency for different concentrations of B+Bz for corrosion of C38 steel in 3% NaCl.

| Conc. (M) B+BZ | $R_s$ ($\Omega\cdot cm^2$) | $Q_1\cdot10^{-3}$ ($s^n\Omega^{-1}\cdot cm^{-2}$) | $\eta_1$ | $R_1$ ($\Omega\cdot cm^2$) | $C_1$ $\mu F\cdot cm^{-2}$ | $Q_2$ ($s^n\Omega^{-1}\cdot cm^{-2}$) | $\eta_2$ | $R_2$ ($\Omega\cdot cm^2$) | $C_2$ ($10^{-3}\cdot F\cdot cm^{-2}$) | $R_p = R_1+R_2$ | $E$% |
|---|---|---|---|---|---|---|---|---|---|---|---|
| Blank | 10.56 | 0.365 | 0.861 | 49.45 | 192 | 0.015 | 0.699 | 27.19 | 10.48 | 76.66 | – |
| $10^{-4}$ | 10.27 | $6.91\cdot10^{-2}$ | 0.770 | 248.2 | 20.6 | 0.049 | 0.496 | 152.2 | 0.379 | 400.4 | 80.85 |
| $10^{-3}$ | 10.65 | $7.20\cdot10^{-2}$ | 0.787 | 276.5 | 24.9 | 0.049 | 0.668 | 172.7 | 0.143 | 449.2 | 82.94 |
| $5\cdot10^{-3}$ | 10.27 | $7.56\cdot10^{-2}$ | 0.728 | 401.6 | 20.6 | 0.017 | 0.574 | 214.9 | 0.0439 | 616.5 | 87.4 |

$$IE(\%) = \left(1 - \frac{R_t}{R_{t(inh)}}\right)\cdot 100 \quad (4)$$

where $R_t$ and $R_{t(inh)}$ are respectively the total resistance ($R_t = R_1 + R_2$) in the absence and in the presence of the extract.

The "double layer capacitance" values ($C_{dl}$) were calculated using the parameters fitting the diagrams to the equation 5 [24].

$$C_{dl} = \left(Q\cdot R_t^{1-\eta}\right)^{1/\eta} \quad (5)$$

From Table 4, it can be seen that the $R_s$ values remain almost unchanged upon addition of inhibitor. The $R_1$ and $R_2$ values increase with the inhibitor concentration. Consequently, the total resistance ($R_t = R_1 + R_2$) increases with the inhibitor concentration, leading to an increase in the corrosion inhibition efficiency. The $IE$(%) values calculated from impedance study are in agreement with those obtained from polarization measurements.

The first phenomenon, the decrease of $C_1$ is not as regular as the first one. We can suppose that the passive layer is porous [25, 27, 28]. According to Mouangua [25] and Muster [26], the corrosion layer is porous and hydrated as observed in SEM micrographs, in the same way, XPS studies showed that the zinc hydroxide chloride is the dominant corrosion products. The decrease in the CPE parameters $Q$ with increase in inhibitor concentrations confirms the formation of a protective layer covers the zinc surface and an increase in the corrosion inhibition.

The decrease of the $C_2$ of the second phenomenon could be attributed to the adsorption of the inhibitors on the electrode surface forming protective adsorption layers. The double

layer capacitance occurs at the electrode/electrolyte interface. The electrode surface has a charge, due to an excess or depletion of electrons, which resides with the atoms in the first layer of the surface and is balanced by an equal number of oppositely charged particles in the electrolyte. The distribution of this charge determines the field strength of the interface, which, in turn, defines the speed of ion transfer. The decrease of capacitance is due to the displacement of water molecules and other ions originally adsorbed on the electrode by the inhibitor molecules, forming a protective layer, which decrease the number of actives sites necessary for the corrosion reaction and so increase corrosion inhibition.

## Conclusion

In this work, we successfully synthesized the surfactant (B+Bz). The NMR, IR, mass spectrum and microanalysis characterizations fully confirm the chemical structure of the surfactant.

To examine the anticorrosion ability of the synthesized surfactant on metallic surfaces, gravimetric and Kesternich tests were performed on zinc in 3% NaCl. Those tests showed that the inhibitor B+Bz showed very good inhibiting efficiency.

Electrochemical studies demonstrated a shift of potential towards more negative values and a diminution of the current densities. Therefore, we have a mixed inhibitor. A higher concentration of inhibitor leads to an increase in the inhibitory effectiveness of zinc in the 3% NaCl solution.

Anticorrosion ability of different types of surfactants can be potentially used in the industry as good options to solve the problems of corrosion on metallic surfaces in order to prevent the material and economic loss.

Analysis by impedance spectroscopy shows that $R_t$ values increase, while the values of $C_{dl}$ decrease. Change in $C_{dl}$ is likely due to the adsorption of organic molecules onto the metal surface, decreasing the rate of dissolution reactions.

## References

1. A.A. Al-Amiery, A. Kadhim, A. Al-Adili and Z.H. Tawfiq, Limits and developments in ecofriendly corrosion inhibitors of mild steel: A critical review. part 1: Coumarins, *Int. J. Corros. Scale Inhib.*, 2021, **10**, no. 4, 1355–1384. doi: 10.17675/2305-6894-2021-10-4-1
2. M. Rosen and J. Kunjappu, *Surfactants and interfacial phenomena*, John Wiley & Sons, Inc., Hoboken, New Jersey, 2012.
3. B. David, P. Jordan and D.R. Kara, Industrial Applications of Surfactants, *Cambridge: Royal Society of Chemistry*,1990, **2**, 195–216.
4. R.A. Stephenson and D.R. Karsa, Industrial Applications of Surfactants, *Cambridge: Royal Society of Chemistry*,1990, **2**, 235–275.
5. E.J.R. Sudholter, J.B. Engberts and W.H. De Jeu, Thermotropic liquid-crystalline behavior of some single-and double-chained pyridinium amphiphiles, *J. Phys. Chem.*, 1982, **86**, 1908–1913. doi: 10.1021/j100207a035

6. G. Ronsin, C. Perrin, P. Guédat, A. Kremer, P. Camilleri and A.J. Kirby, Novel spermine-based cationic gemini surfactants for gene delivery, *Chem. Commun*., 2001, **21**, 2234–2235. doi: 10.1039/B105936J
7. A.D. James, D. Stewart and D.R. Karsa, Industrial Applications of Surfactants, *Cambridge: Royal Society of Chemistry*,1990, **2**, 338–355.
8. F.J. Kenny and D.R. Karsa, Industrial Applications of Surfactants, *Cambridge: Royal Society of Chemistry*,1990, **2**, 366–394.
9. X. Zhou, H. Yang and F. Wang, Investigation on the inhibition behavior of a pentaerythritol glycoside for carbon steel in 3.5% NaCl saturated $Ca(OH)_2$ solution, *Corros. Sci*., 2012, **54**, 193–200. doi: 10.1016/j.corsci.2011.09.018
10. A.Al Maofari, G. Ezznaydy, Y. Idouli, F. Guédira, S. Zaydoun, N. Labjar and S. El, Inhibitive action of 3,4'-bi-1,2,4-Triazole on the corrosion of copper in NaCl 3% solution, *J. Mater. Environ. Sci*., 2014, **5**, 2081–2085.
11. R.H. Jin and T. Nishikubo, New Ring Opening Reaction of Epoxides With Chloro-Substituted Aromatic and Heteroaromatic Compounds, *Synthesis*, 1993, **01**, 28–30. doi: 10.1055/s-1993-25780
12. A.R. Katritzky, R.J. Offerman and Z. Wang, Utilization of pyridinium salts as microsensor coatings, *Langmuir*, 1989, **5**, no. 4, 1087–1092. doi: 10.1021/la00088a036
13. A. Sayari, Catalysis by crystalline mesoporous molecular sieves, *Chem. Mater*., 1996, **8**, no. 8, 1840–1852. doi: 10.1021/cm950585+
14. D.N. Rubingh and P.M. Holland, *Physical chemistry*, Marcel Dekker, New York, 1991.
15. M.S. Borse and S. Devi, Importance of head group polarity in controlling aggregation properties of cationic gemini surfactants, *Adv. Colloid Interface Sci*., 2006, **123–126**, 387–399. doi: 10.1016/j.cis.2006.05.017
16. M. El Achouri, M.R. Infante, F. Izquierdo, S. Kertit, H.M. Gouttaya and B. Nciri, Synthesis of some cationic gemini surfactants and their inhibitive effect on iron corrosion in hydrochloric acid medium, *Corros. Sci*., 2001, **43**, no. 1, 19–35. doi: 10.1016/S0010-938X(00)00063-9
17. Y.K. Leong, P.I. Au and P. Clode, Microstructure of KGa-1b and KGa-2 kaolin suspensions revisited, *Colloids Surf., A*, 2021, **617**, 126–354. doi: 10.1016/j.colsurfa.2021.126354
18. N. Hajjaji, I. Rico, A. Srhiri, A. Lattes, M. Soufiaoui and A.B. Bachir, Effect of *N*-alkylbetaines on the corrosion of iron in 1 M HCl solution, *Corrosion*, 1993, **49**, no. 4, 326–334. doi: 10.5006/1.3316057
19. H. Ma, S. Chen, S. Zhao, X. Liu and D. Li, A study of corrosion behavior of copper in acidic solutions containing cetyltrimethylammonium bromide, *J. Electrochem. Soc*., 2001, **148**, B482. doi: 10.1149/1.1409543
20. M.M. Osman, R.A. El-Ghazwan and A.M. Al-Sabagh, Corrosion inhibitor of some surfactants derived from maleic-oleic acid adduct on mild steel in 1 M $H_2SO_4$, *Mater. Chem. Phys*., 2003, **80**, no. 1, 55–62. doi: 10.1016/S0254-0584(01)00588-0

21. J. Pereira-Lachataignerais, R. Pons, P. Panizza, L. Coubin, J. Rouch and O. Lopez, Study and formation of vesicle systems with low polydispersity index by ultrasound method, *Chem. Phys. Lipids*, 2006, **140**, no. 1–2, 88–97. doi: 10.1016/j.chemphyslip.2006.01.008
22. H. Saufi, A. Al Maofari, A. El Yadin, L. Eddaif, H. Harhar, S. Gharby and S. El Hajjaji, Evaluation of vegetable oil of nigel as corrosion inhibitor for iron in NaCl 3% medium, *J. Mater. Environ. Sci*., 2015, **6**, no. 7, 1845–1849.
23. M. Mouanga and P. Berçot, Comparison of corrosion behaviour of zinc in NaCl and in NaOH solutions; Part II: Electrochemical analyses, *Corros. Sci*., 2010, **52**, no. 12, 3993–4000. doi: 10.1016/j.corsci.2010.08.018
24. N. Labjer, M. Lebrini, F. Bentiss, N.E. Chihib, S. El Hajjaji and C. Jama, Corrosion inhibition of carbon steel and antibacterial properties of aminotris-(methylenephosphonic) acid, *Mater. Chem. Phys*., 2010, **119**, no. 1–2, 330–336. doi: 10.1016/j.matchemphys.2009.09.006
25. M. Mouanga, P. Berçot and J.Y. Rauch, Comparison of corrosion behavior of zinc in NaCl and in NaOH solutions. Part I: Corrosion layer characterization, *Corros. Sci*., 2010, **52**, no. 12, 3984–3992. doi: 10.1016/j.corsci.2010.08.003
26. N.M. El Basiony, E.E. Bader, S.A. Baker and A.S. El-Tabei, Experimental and theoretical (DFT&MC) studies for the adsorption of the synthesized Gemini cationic surfactant based on hydrazide moiety as X-65 steel acid corrosion inhibitor, *Appl. Surf. Sci*., 2021, **539**, 148246. doi: 10.1016/j.apsusc.2020.148246
27. I. Campos, M. Palomar-Pardavé, A. Amador, C.V. Velázquez and J. Hadad, Corrosion behavior of boride layers evaluated by the EIS technique, *Appl. Surf. Sci*., 2007, **253**, no. 20, 9061–9066. doi: 10.1016/j.apsusc.2007.05.016
28. D. Wang, Y. Li, B. Chen and L. Zhang, Novel surfactants as green corrosion inhibitors for mild steel in 15% HCl: experimental and theoretical studies, *Chem. Eng. J*., 2020, **402**, 126219. doi: 10.1016/j.cej.2020.126219

♦ ♦ ♦